中国科学院近代物理研究所
Institute of Modern Physics, Chinese Academy of Sciences

Surface-Driven Field Emission Mechanisms and Mitigation in SRF Cavities

Tongtong Zhu, Ming Lu, Andong Wu, Tiancai Jiang,Teng Tan and Yuan He

(On behalf of SRF group)

Linac Centre, Institute of Modern Physics, CAS

2026·6·11

Outline

1.1 Background

- In recent years, superconducting radio-frequency (SRF) technology has been widely implemented in major accelerator facilities, such as CiADS, HIAF, SHINE, HEPS, CSNS, among others.

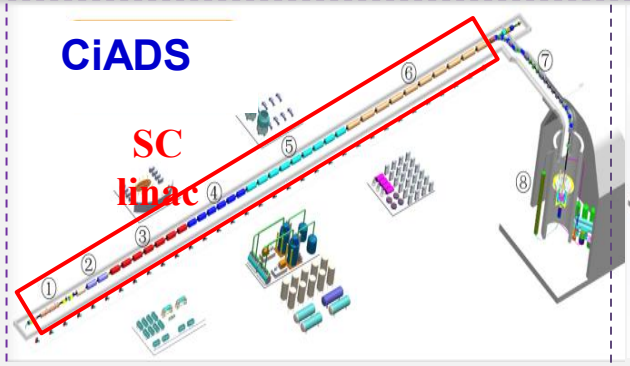

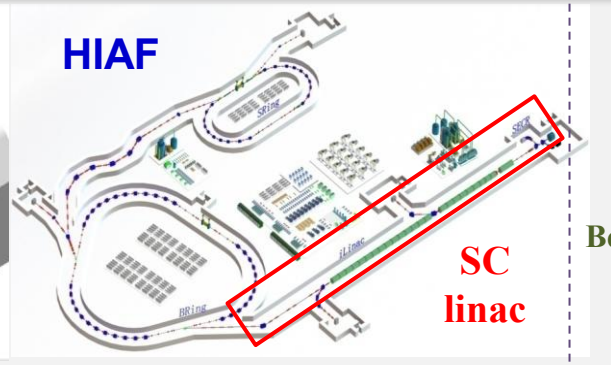

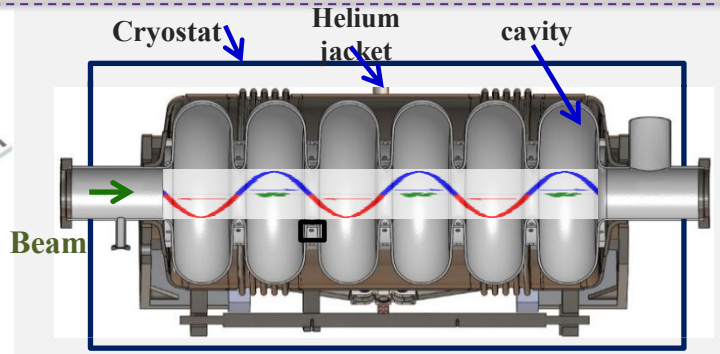

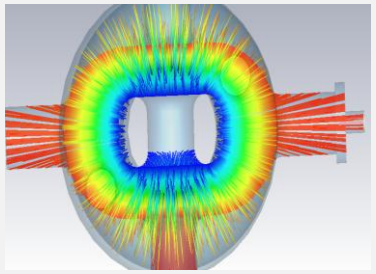

Field emission

The field emission effect is the core factor limiting high-gradient stable operation of SRF cavities.

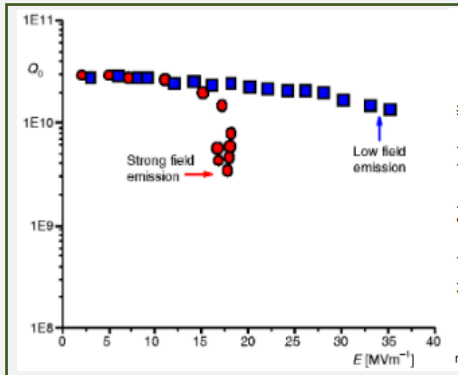

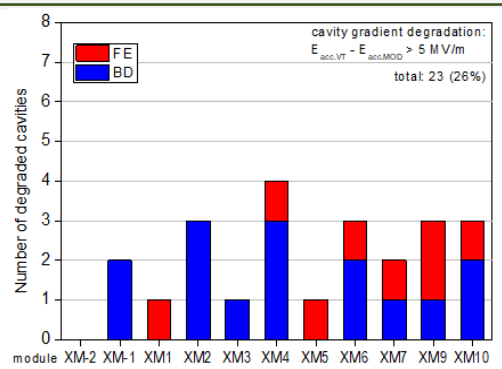

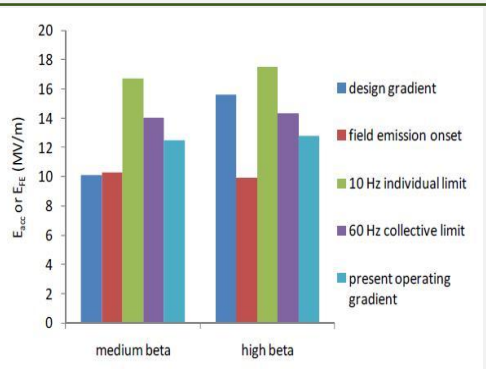

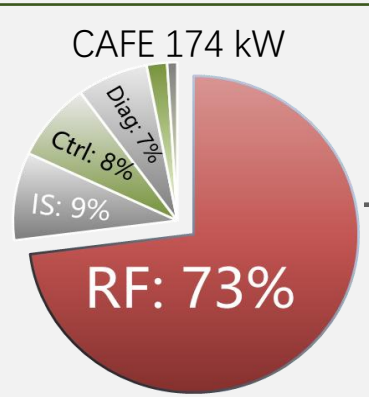

Heat load ↑

Vacuum load↑

Dark current load ↑

Steady-state

Transient

Field-emission-induced degradation of accelerating gradient and quality factor during extended operation remains a global challenge, resulting in sustained performance decline of SRF cavities

1.2 Background

- **Residual gas adsorption on the surface and carbide contamination are important factors contributing to the performance degradation of SRF cavities.**

Performance Degradation and Recovery Induced by Residual Gas Adsorption in Vacuum

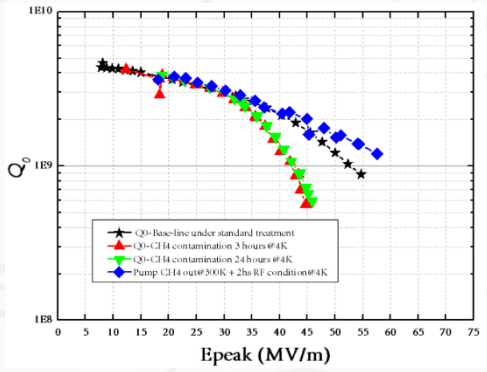

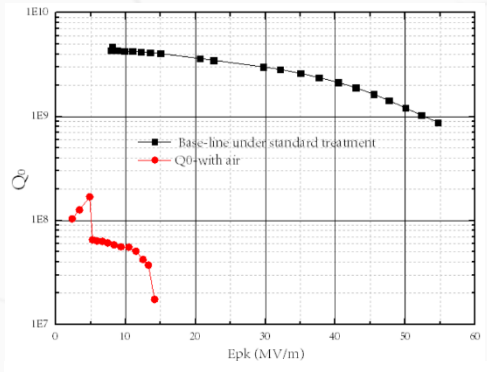

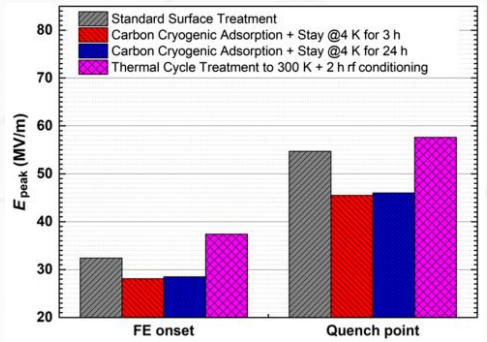

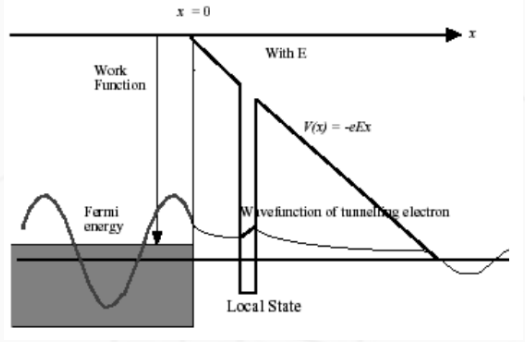

Research status: It has been demonstrated that adsorption of gases such as air and methane causes severe performance degradation.
Treatment methods: Thermal cycling and RF conditioning.
Existing problems: Vacuum residual gas comprises multiple gas species. The adsorption mechanisms of different gases on the surface and their respective effects on field emission remain unclear.

Performance Degradation and Recovery Induced by Surface Carbide Contamination

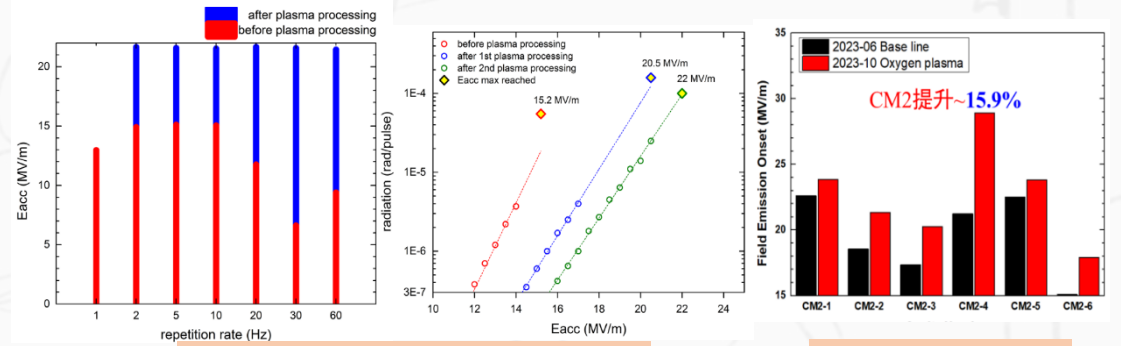

SNS 6-cell SRF cavity

CAFE

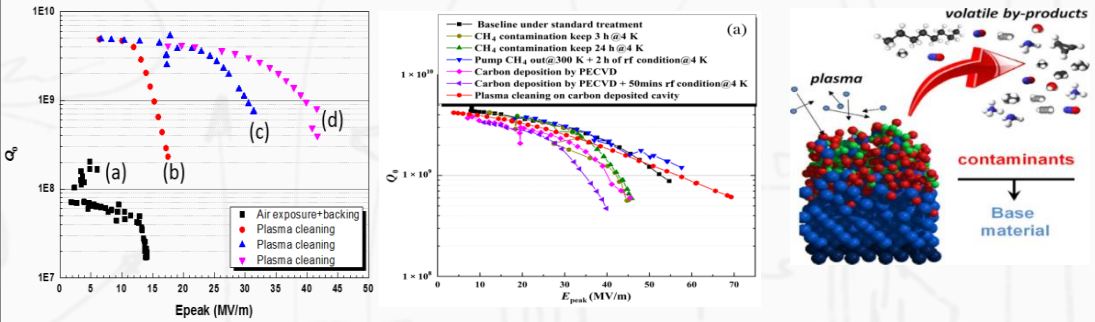

Research status: It has been demonstrated that oxygen plasma cleaning can effectively restore the performance of carbon-contaminated superconducting cavities.
Treatment method: Reactive oxygen plasma cleaning.
Existing problems: The selection of process parameters for in-situ plasma cleaning remains empirical and lacks theoretical guidance. A insufficient understanding of plasma characteristics inside superconducting cavities leads to low cleaning efficiency.

2.1 Adsorption of Vacuum Residual Gases on Nb(110)

- Adsorption of O_2 at different sites induces strong interactions among the d, p, and s orbitals of Nb and O atoms, leading to variations in adsorption configuration, adsorption energy, and work function.

Evolution of Surface Structure Following O_2 Adsorption on the Nb(110) Crystal Plane

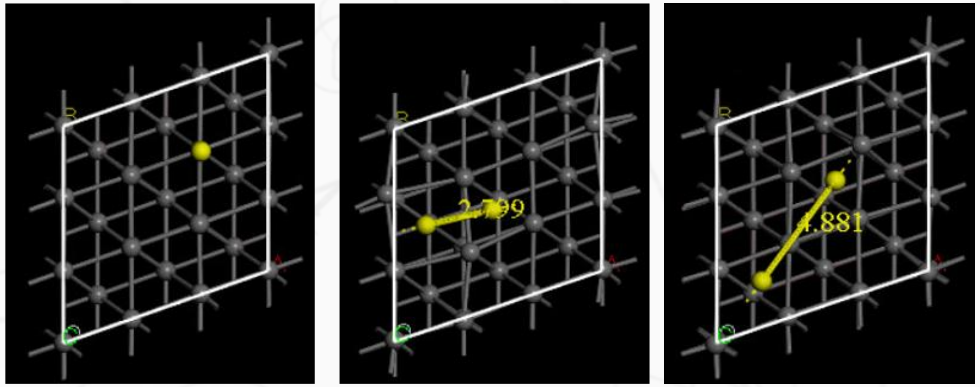

Initial positions: top site, bridge site, hollow site

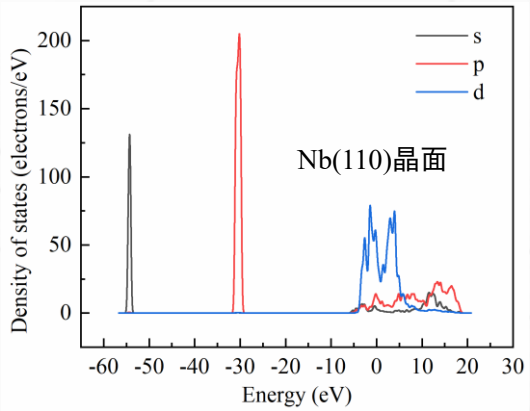

- Initial adsorption at the top site yields a stable post-adsorption structure with the lowest adsorption energy and an increased work function, whereas adsorption at the bridge and hollow sites induces dissociative adsorption and a slight reduction in work function.

Surface Properties of Nb(110) Following O_2 Adsorption: Adsorption Energy, Work Function, and Partial Density of States

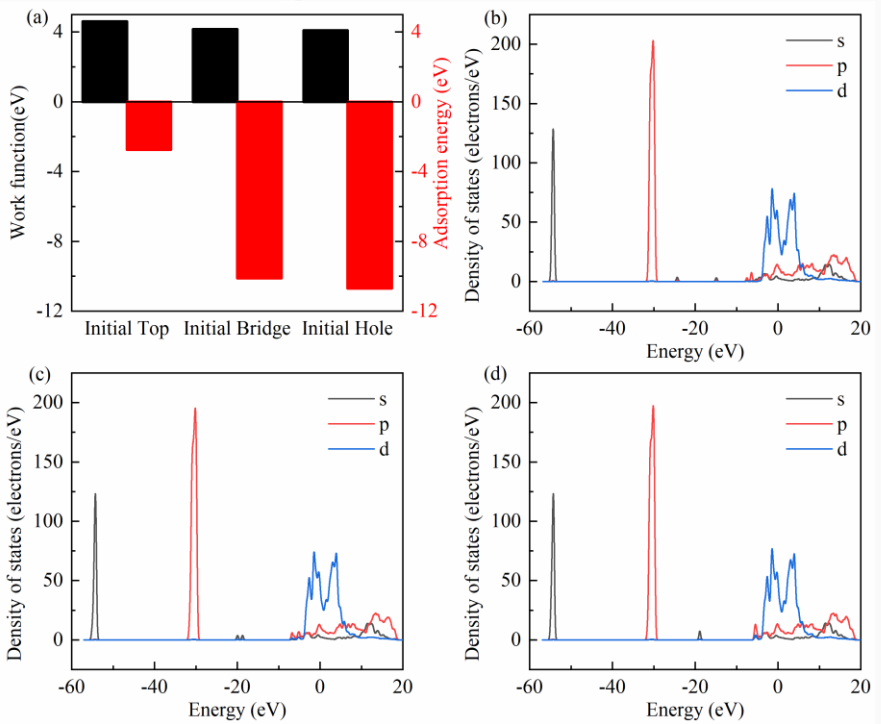

- After O_2 adsorption at different sites, the d orbitals of Nb atoms and the p orbitals of O_2 molecules (or O atoms) first undergo hybridization near −5 eV, followed by hybridization of s orbitals in the range of −14 to −19 eV.

2.2 Adsorption of Vacuum Residual Gases on Nb(110)

- N_2 exhibits a relatively high adsorption energy on the Nb(110) surface but has a minor effect on the work function. In contrast, CO_2 primarily undergoes weak adsorption on the surface, leading to a substantial decrease in the work function.

Surface Properties of N_2 Adsorption on the Nb(110) Crystal Plane

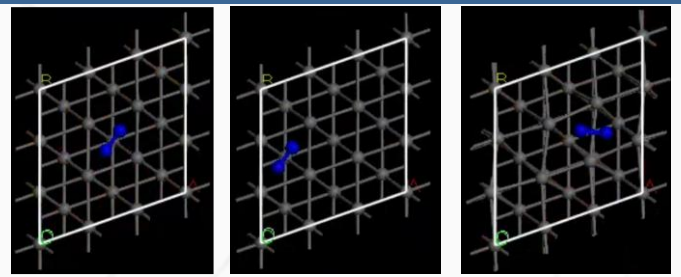

Initial positions: top site, bridge site, hollow site

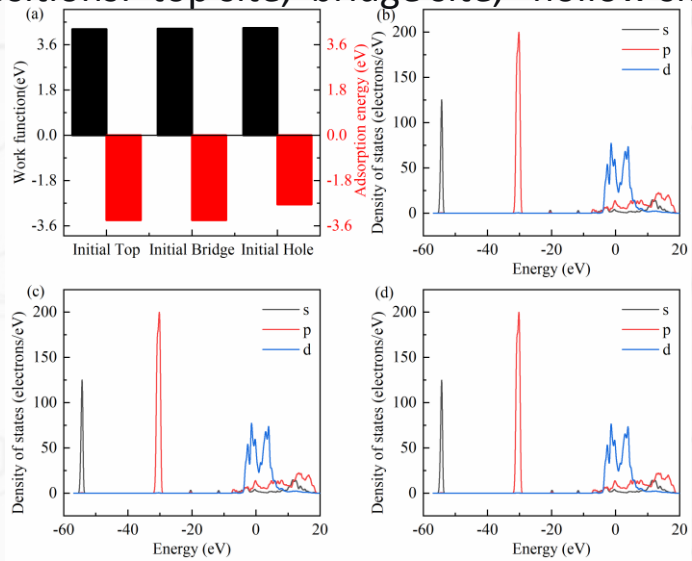

- A weak interaction occurs between the d orbitals of Nb atoms and the p orbitals of N_2 molecules near approximately −7 eV.
- N_2 adsorption on the Nb(110) surface predominantly takes place at hollow sites, and its post-adsorption effect on the work function is negligible.

Surface Properties of CO_2 Adsorption on the Nb(110) Crystal Plane

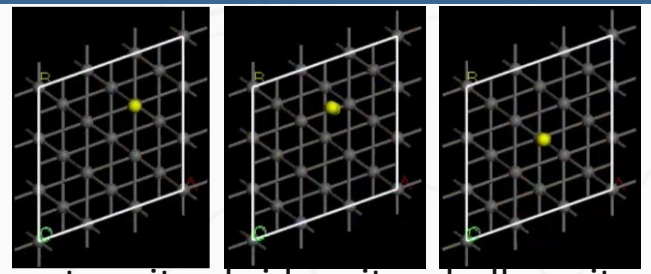

Initial positions: top site, bridge site, hollow site

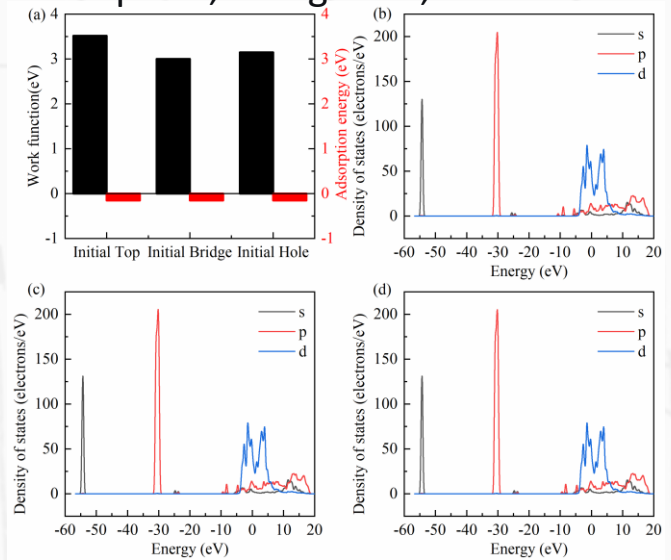

- CO_2 adsorbs weakly on Nb with negligible positional change, a large work function drop, and very low adsorption energy. Strong Nb d–CO_2 p orbital interactions occur at −5–6, −8–10, and −10–11 eV.

2.3 Adsorption of Vacuum Residual Gases on Nb(110)

- CO molecules form strong chemical adsorption on Nb(110) without reducing the surface work function.

Surface Properties of CO Adsorption on the Nb(110) Crystal Plane

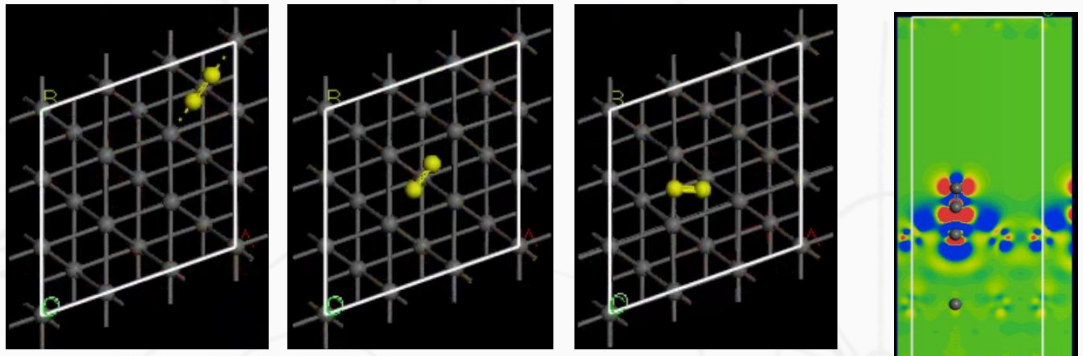

Initial positions: top site, bridge site, hollow site

- After stable adsorption, CO molecules change their orientation from perpendicular to parallel with respect to the surface, and all initially adsorbed species at top, bridge, and hollow sites converge to hollow sites.
- Although CO chemisorbs strongly on Nb(110), it does not lower the work function. Consequently, CO adsorption on Nb(110) does not lead to enhanced field emission.

Surface Properties of CO Adsorption on the Nb(110) Crystal Plane

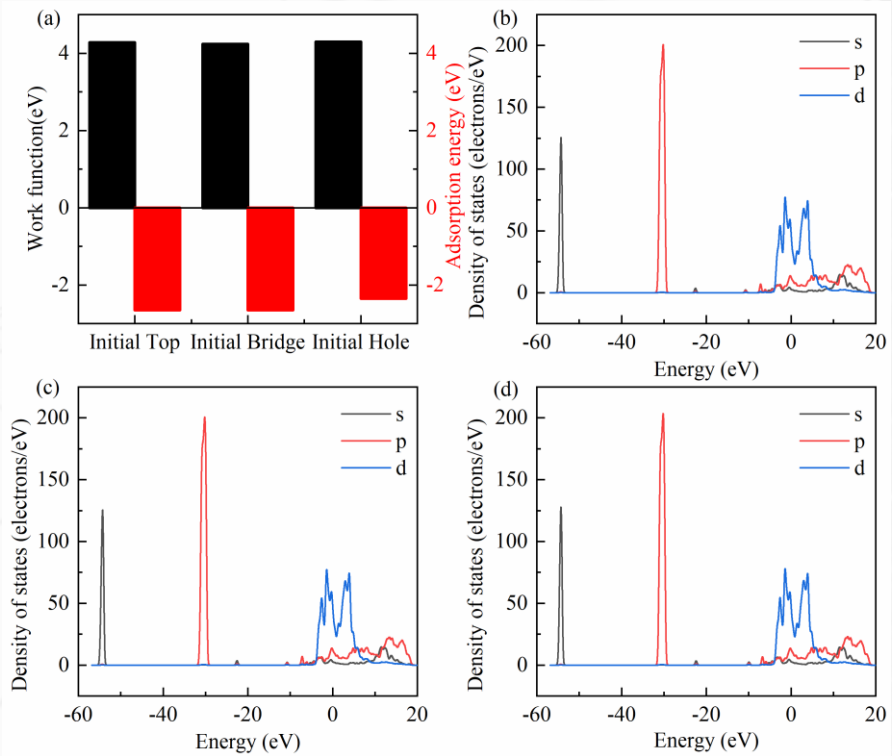

- Strong interactions occur between the d orbitals of Nb atoms and the p orbitals of CO molecules in the energy range of −5 to −8 eV, giving rise to two hybridization peaks of different heights.

2.4 Temperature Dependence of the Adsorption of Vacuum Residual Gas

- The combined effects of thermodynamic characteristics, gas molecular dynamics, and highly active sites on the niobium surface give rise to a "cryopumping" effect on the Nb surface at low temperatures.

Adsorption Characteristics of O_2, N_2, CO, and CO_2 on Niobium Surfaces at Different Temperatures

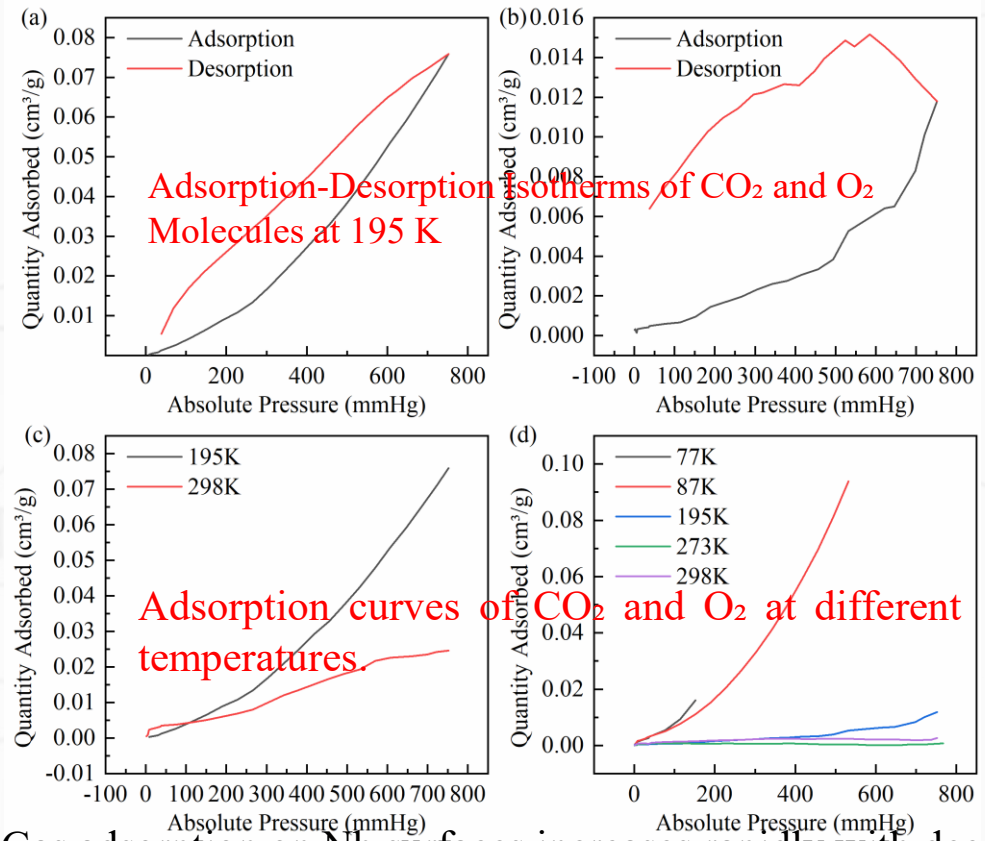

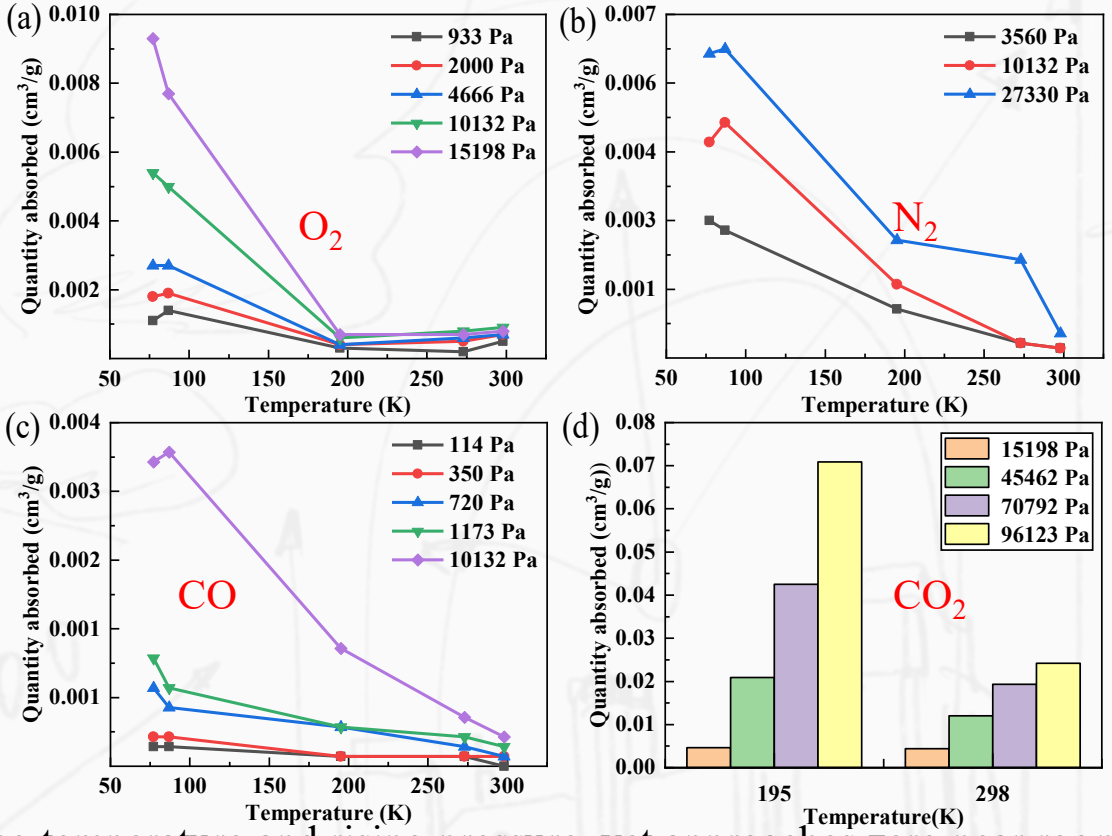

- Gas adsorption on Nb surfaces increases rapidly with decreasing temperature and rising pressure, yet approaches zero near room temperature.
- The adsorption process is dictated by the interplay of adsorption thermodynamics, gas molecular dynamics, and highly active surface sites.

3.1 Kinetic Modeling of Oxygen Plasma Reactions with Hydrocarbons

- A surface reaction kinetic model was constructed incorporating both the chemical action of reactive oxygen plasma with hydrocarbons and the physical action of ion bombardment. The key physical parameters influencing the cleaning process are Fo, V, n_i, and T_e.

Surface Kinetic Modeling of Reactive Oxygen Plasma Reactions with Hydrocarbons

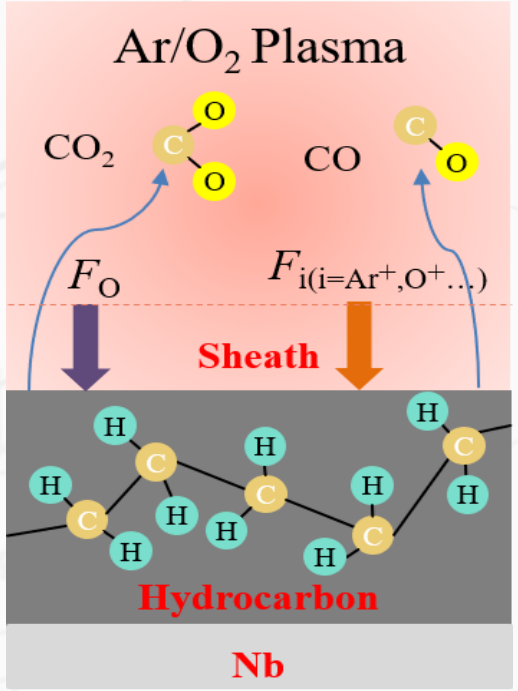

Schematic Diagram of the Reaction of Ar/O_2 Plasma with Hydrocarbons

Ion-enhanced chemical reaction

$$w = \theta \cdot S_o \cdot c_1 \cdot F_o \cdot c_2 \cdot V \cdot \sum F_i \cdot q_{i(i=\mathrm{Ar}^+,\ \mathrm{O}^+\cdots)}$$

$$w = \theta \cdot S_o \cdot c \cdot F_o \cdot V \cdot \sum F_i \cdot q_{i(i=\mathrm{Ar}^+,\mathrm{O}^+\cdots)}$$

Sheath model

$$F_i = n_s \cdot \mu_B$$

$$\mu_B = (e \cdot T_e / M_i)^{1/2}$$

Plasma cleaning rate

$$w = \theta \cdot S_o \cdot c \cdot F_o \cdot V \cdot \sum q_i \cdot 0.6 n_i \cdot \frac{eT_e}{M_i} (i = \mathrm{O}^+、\ \mathrm{Ar}^+ \ldots)$$

Plasma cleaning rate equation

$$w = \theta \cdot S_o \cdot c \cdot F_o \cdot V \cdot \sum q_i \cdot 0.6 n_i \cdot \frac{e'l'_e}{M_i} = (\sum Y_{d,i} \cdot F_i + K_T \cdot \rho_s) \cdot \theta$$

$$= \sum A \cdot (E_i^{0.5} - E_{l,d}^{0.5}) \cdot F_i + K_T^0 \cdot \exp(-\frac{E_{\mathrm{des}}}{k \cdot T_s}) \cdot \rho_s$$

Reaction coefficient

$$c = \frac{\sum A \cdot (E_i^{0.5} - E_{l,d}^{0.5}) \cdot F_i + K_T^0 \cdot \exp(-\frac{E_{des}}{k \cdot T_s}) \cdot \rho_s}{\theta \cdot S_o \cdot F_o \cdot V \cdot \sum q_i \cdot 0.6 n_i \cdot \frac{eT_e}{M_i}}$$

The formation of chemical products is consistent with thermal desorption and ion-stimulated desorption.

$$w = \theta \cdot S_o \cdot c \cdot F_o \cdot V \cdot \sum q_i \cdot 0.6 n_i \cdot \frac{e'l'_e}{M_i} = (\sum Y_{d,i} \cdot F_i + K_T \cdot \rho_s) \cdot \theta$$

$$K_T = K_T^0 \exp(-\frac{E_{des}}{kT_s}) \qquad Y_d = A \cdot (E_i^{0.5} - E_{l,d}^{0.5})$$

3.2 Spatial Distribution of Reactive Oxygen Species in an ICP Plasma

- Spatial distributions and temporal evolutions of key parameters (electron density, electron temperature, plasma potential, and O-atom density) inside an ICP reactor were obtained using a plasma fluid model.

Fluid Simulation of an Inductively Coupled Plasma (ICP) Source

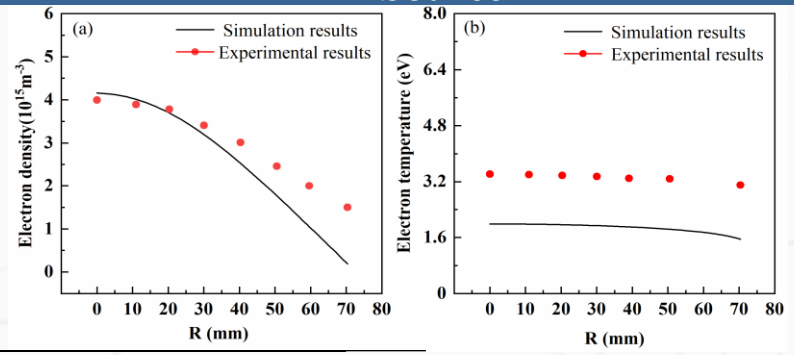

No.	Reaction	Rate coefficient /cm^3·s^{-1}	E_e/eV
1	e + O_2 →e + O_2	$4.7\times10^{-8}T_e^{0.5}$	$3T_e(m_e/m_n)$
2	e + O_2 →O^- + O	$8.8\times10^{-11}\exp(-4.4/T_e)$	3.637
3	e + O_2 →e + 2O	$4.2\times10^{-9}\exp(-5.6/T_e)$	6.4
4	e + O_2 →2e + O_2^+	$9.0\times10^{-10}T_e^{0.5}\exp(-12.6/T_e)$	12.6
5	e + O^- →2e + O	$2.0\times10^{-7}\exp(-5.5/T_e)$	5.5
6	e + O_2^+ →2O	$5.2\times10^{-9}/T_e$	-6.96
7	e + O_2 →e + O^- + O^+	$7.1\times10^{-11}T_e^{0.5}\exp(-17/T_e)$	17
8	e + O_2 →2e + O + O^+	$5.3\times10^{-10}T_e^{0.9}\exp(-20/T_e)$	20
9	e + O→2e + O^+	$9.0\times10^{-9}T_e^{0.7}\exp(-13/T_e)$	13
10	e + O_2 →e + O_2*	$1.7\times10^{-9}\exp(-3.1/T_e)$	0.98
11	e + O_2* →e + O_2	$5.6\times10^{-9}\exp(-2.2/T_e)$	-0.98
12	e + O_2*→O+ O	$2.28\times10^{-10}\exp(-2.29/T_e)$	5.19
13	e + O_2 →O + O* + e	$5\times10^{-8}\exp(-8.4/T_e)$	8.57
14	e + O→O* + e	$4.2\times10^{-9}\exp(-2.25/T_e)$	1.97
15	e + O*→e + O	8×10^{-9}	-1.97
16	e + O*→O^+ + 2e	$9.0\times10^{-9}T_e^{0.7}\exp(-11.6/T_e)$	11.6
17	e + O_2* →2e + O_2^+	$9.0\times10^{-9}T_e^{2}\exp(-11.6/T_e)$	11.08
18	e + O_2*→2O + e	$4.2\times10^{-9}\exp(-4.6/T_e)$	5.42
19	e + O_2*→O + O* + e	$2.04\times10^{-8}\exp(-7.4/T_e)$	7.59
20	e + O_2*→O + O^+ + 2e	$5.3\times10^{-10}T_e^{0.9}\exp(-19/T_e)$	17.7
21	e + Ar →e + Ar^+	BE	15.6
22	O^- + O_2^+ →O_2 + O	1×10^{-7}	-
23	O^- + O →O_2 + e	3×10^{-10}	-
24	O^- + O_2^+ →3O	1×10^{-7}	-
25	O^- + O^+ →2O	$2.7\times10^{-7}(300/T_n)^{0.5}$	-
26	O^+ + O_2 →O_2^+ + O	$2\times10^{-11}(300/T_n)^{0.5}$	-
27	O_2* +O_2 →2O_2	$2.8\times10^{-18}(300/T_n)^{0.8}$	-
28	O_2* + O→O_2 + O	2×10^{-16}	-
29	O* + O→2O	8×10^{-12}	-
30	O* + O_2 →O + O_2	$7\times10^{-12}\exp(67/T_n)$	-
31	O* + O_2 →O + O_2*	1×10^{-12}	-

- Five charged species (e, O^+, O^-, O_2^+, Ar^+), two excited species (O_2, *O*), and three ground-state species (O_2, O, Ar) were considered, involving 31 reactions including elastic scattering, desorption, recombination, ionization, dissociative attachment, and charge exchange.

Spatial Distribution of Reactive Species in an ICP Reactor

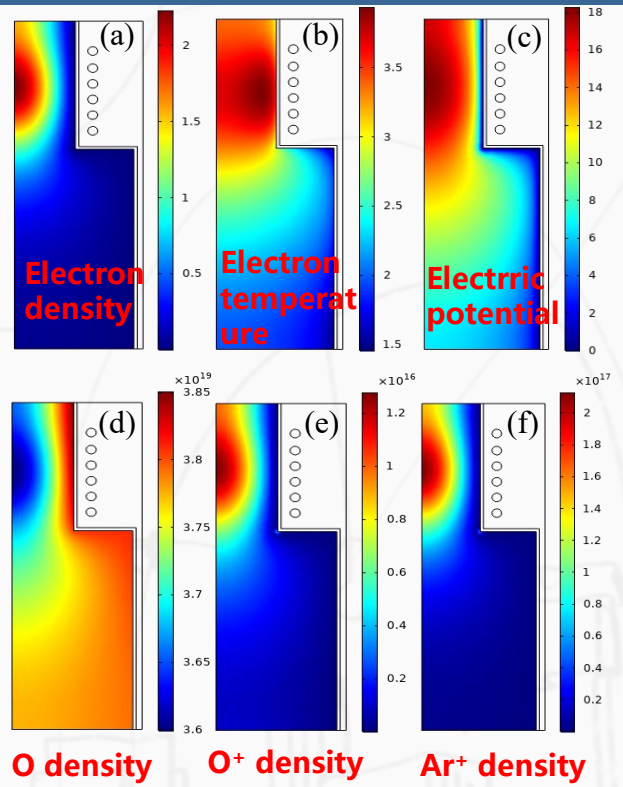

- The electron density reaches a maximum of 2.2 × 10^{17} m^{-3} near the RF coil, with a peak electron temperature of 3.8 eV and a plasma potential of 18 V.
- The O-atom density is lower in the central region of the quartz tube near the coil and becomes higher and more uniform near the quartz tube wall and in the lower part of the reactor.

3.3 Influence of Cleaning Parameters on C/O Content and Oxide Thickness

- The surface carbon content decreases rapidly within the first 60 minutes of cleaning. However, extending the cleaning time beyond this period does not lead to a further reduction in carbon content; instead, it results in a continuous increase in oxide thickness.

XPS Analysis of Surfaces After Different Cleaning Durations

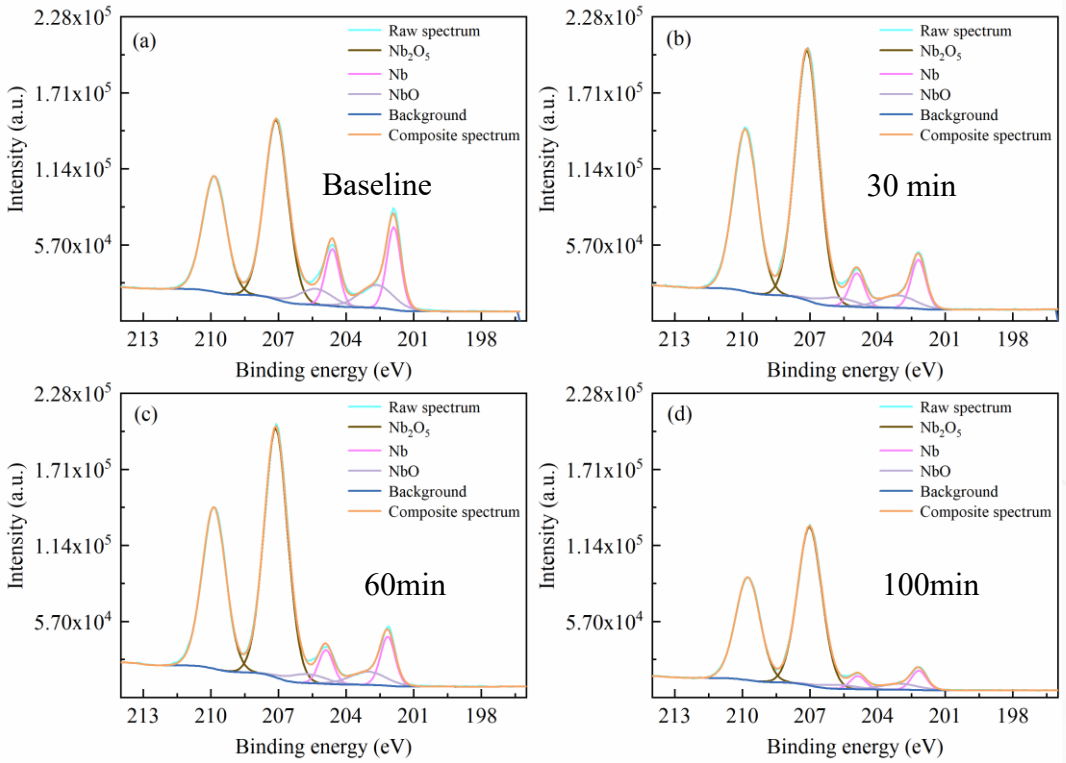

- The surface consists mainly of Nb_2O_5 with minor amounts of NbO, though their relative contents vary. The oxide film thickness can be determined from the Nb_2O_5 and Nb contents.

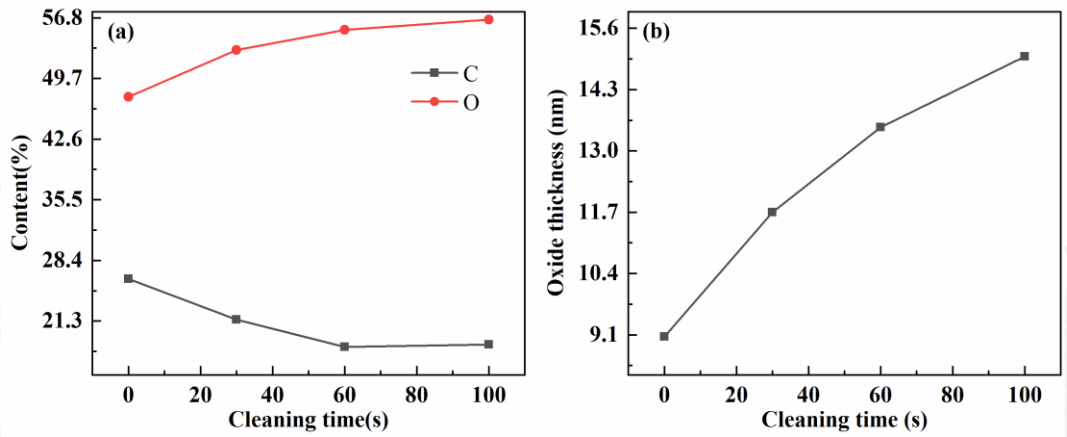

- During the first 60 minutes of plasma cleaning, the carbon content on the Nb surface drops rapidly while the oxygen content increases quickly, driven by a high reaction rate between surface oxygen atoms and carbides along with rapid oxidation by plasma reactive species.
- Extending the cleaning time beyond 60 minutes results in little further reduction in carbon or carbide content but instead leads to a progressive thickening of the surface oxide layer.

Evolution of Surface Composition with Cleaning Time

3.4 Influence of Cleaning Parameters on C/O Content and Oxide Thickness

- Although increasing power enhances the O-atom density, a threshold effect imposes an upper limit on the achievable cleaning rate.

XPS Analysis of Surfaces at Different Powers and Oxygen Concentrations

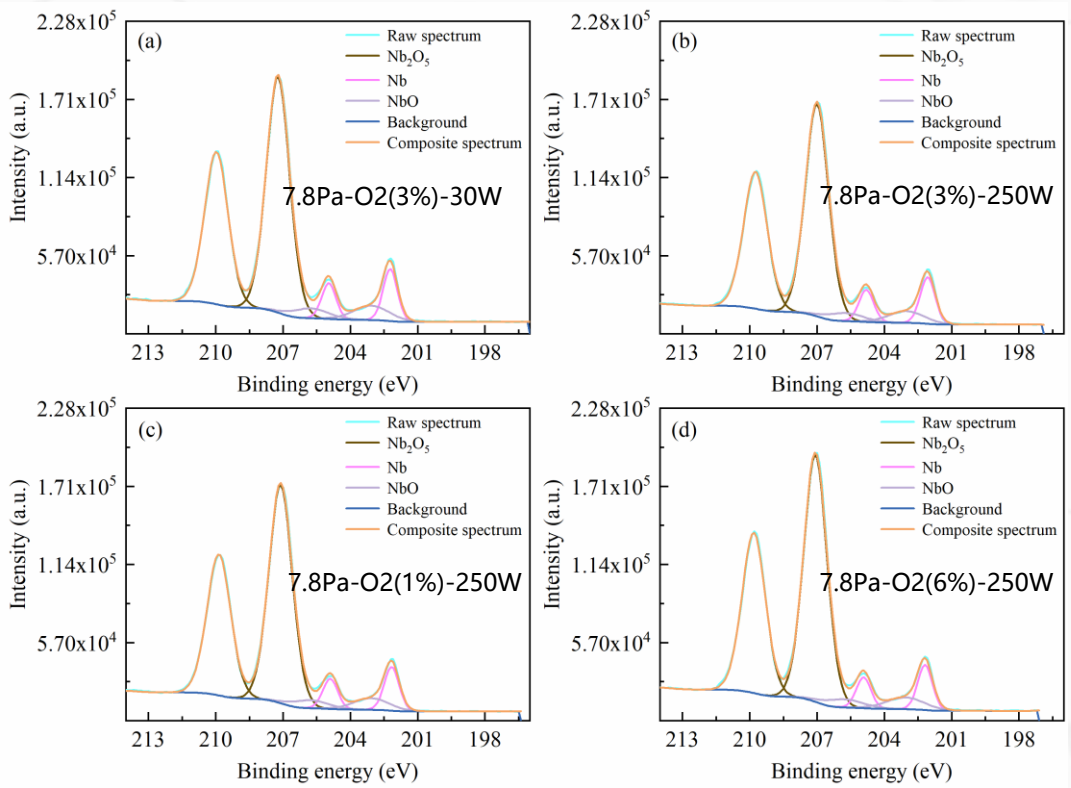

- Surfaces cleaned under varying RF powers and O_2 concentrations exhibit consistent chemical compositions, dominated by Nb_2O_5 and Nb with minor NbO.

Evolution of Surface Composition and Plasma Reactive Species with Varying Power

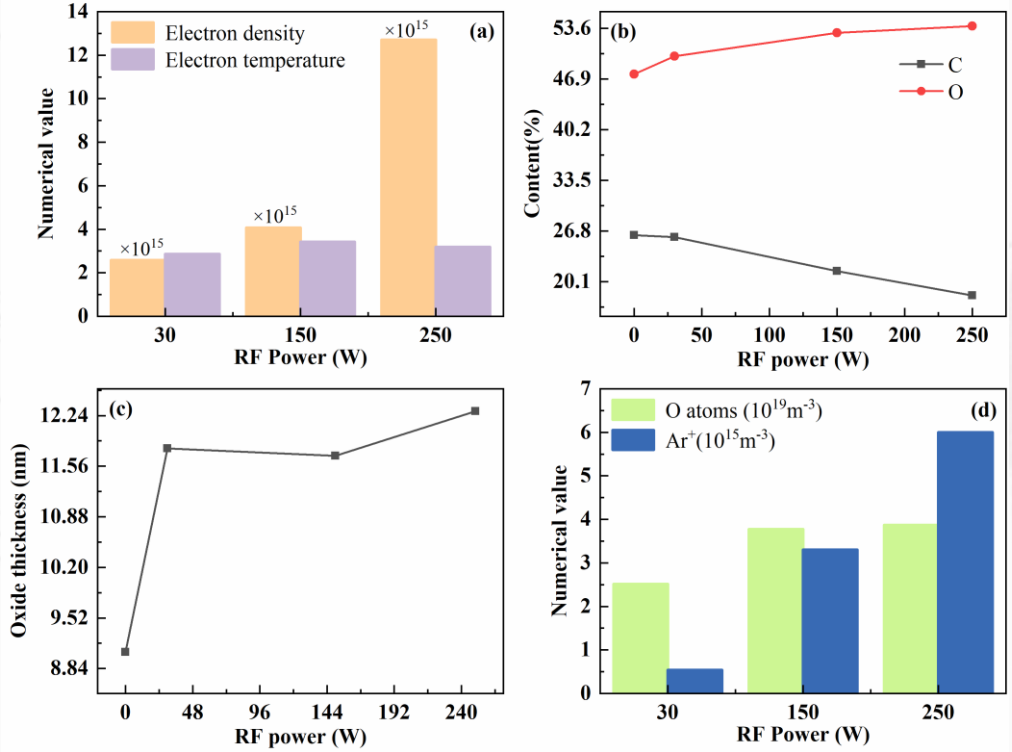

- As the power increases, the electron density rises continuously. The O-atom density increases substantially at lower powers but tends to saturate at higher powers. Consequently, the cleaning rate first increases rapidly and then remains constant, whereas the oxide thickness increases monotonically.

3.5 Influence of Cleaning Parameters on C/O Content and Oxide Thickness

- Increasing the O_2 content leads to a rapid increase in the cleaning rate, while the oxide thickness remains largely unchanged. A decrease in gas pressure results in an increase in O-atom density, which in turn enhances the cleaning rate.

Evolution of Surface Composition and Plasma Reactive Species with Varying O_2 Content

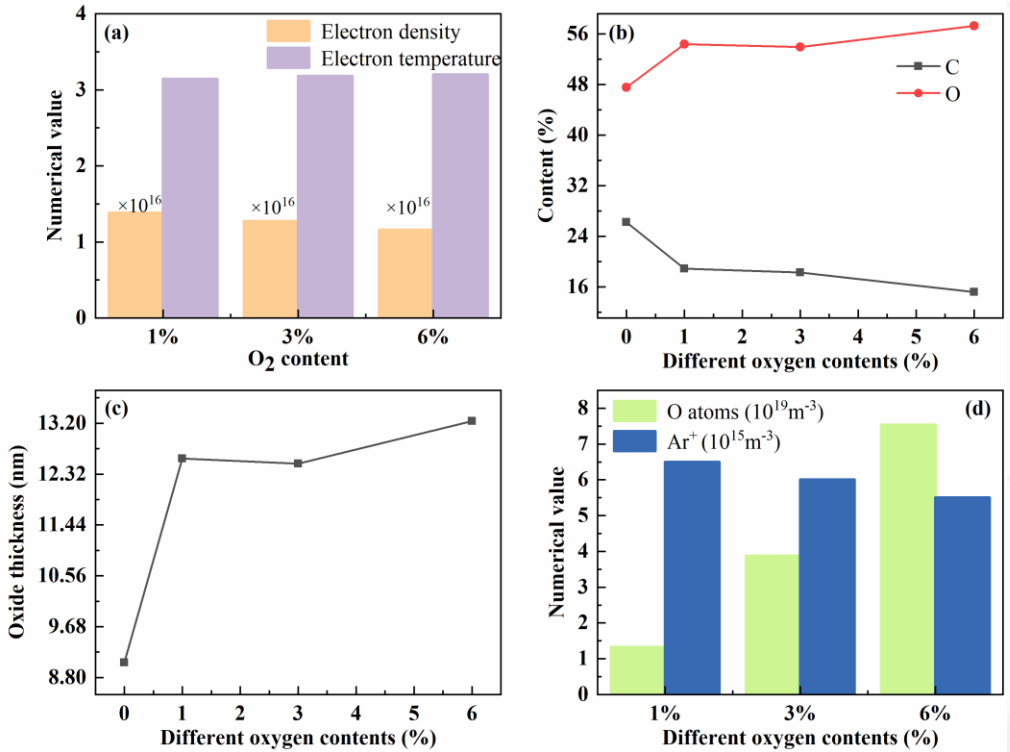

- As the O_2 content increases, the electron density and temperature remain unchanged, while the Ar^+ density continuously decreases and the O-atom density gradually increases. This leads to a rapid increase in the cleaning rate, a further reduction in carbide content from 18% to 15%, and an increase in surface oxide thickness of only 1 nm.

Evolution of Surface Composition and Plasma Reactive Species with Varying gas pressure

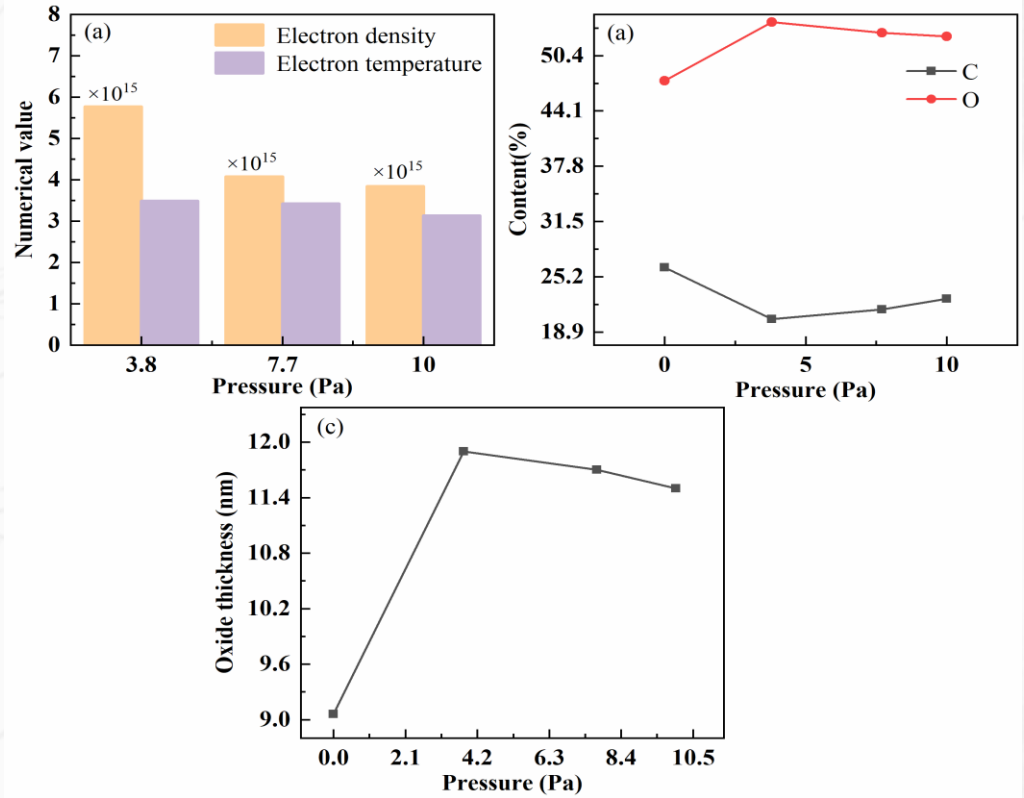

- A decrease in gas pressure leads to an increase in electron density but leaves electron temperature unchanged, accompanied by a reduction in surface carbon content and increases in both oxygen content and oxide thickness.

4 Summary

- Among the gases studied, O_2 exhibits the highest adsorption energy on Nb(110), followed by N_2, whereas CO and CO_2 show the lowest. N_2 and CO adsorption leaves the work function nearly unchanged, whereas CO_2 significantly reduces it, making CO_2 the most detrimental adsorbate responsible for performance degradation in superconducting radio-frequency cavities.
- A surface reaction kinetic model for reactive oxygen plasma with hydrocarbons was constructed, identifying Fo, V, n_i, and T_e as the core physical parameters governing the cleaning process. The effects of cleaning time, power, pressure, and O_2 content on the cleaning rate and surface oxide thickness were elucidated.
- A multivariable synergistic control strategy (power, O_2 content, and pressure) with reduced cleaning time is proposed to suppress excessive oxide growth while maintaining cleaning efficiency. These findings provide quantitative guidance for in-situ plasma cleaning of SRF cavities.

Thanks for your attention !

Question?

2251898001@qq.com